IMA Journal of Applied Mathematics (2015) **80**, 533–553
doi:10.1093/imamat/hxt048
Advance Access publication on 23 January 2014

Sharp Fickian fronts in conjugated polymer films

D. A. Edwards
Department of Mathematical Sciences, University of Delaware, Newark, DE 19716-2553, USA
edwards@math.udel.edu

[Received on 8 January 2013; revised on 20 August 2013; accepted on 10 December 2013]

Many electrochemical devices are formulated on conjugated polymer films. A model is presented for electrogenerated chemiluminescence in such systems. The resulting diffusion equation for ion transport has a standard Fickian form, but with a highly nonlinear diffusion coefficient. The asymptotic analysis of the equation involves both intermediate layers and logarithmic matching. The asymptotic results show a sharp Fickian front, and compare favourably with numerical simulations and experimental results. Additional results are also presented for the solution beyond saturation, as well as in the more realistic case of polar coordinates.

Keywords: asymptotics; electrogenerated chemiluminescence; Fickian diffusion; polymer films; sharp fronts.

1. Introduction

A *conjugated polymer* is one with alternating single and multiple bonds, which causes the delocalization of the π-valence band (polyacetylene is a typical example) (Barford, 2005). A conjugated polymer film can be created by doping the polymer during oxidation and reduction processes (Guo *et al.*, 2011). The delocalization of the valence electrons gives these polymer films desirable electrical properties.

In recent years, the applications of electrochemical conjugated polymer films have multiplied. Such films are used in many types of chemical, humidity and biosensors (Adhikari & Majumdar, 2004). These films can be used in electrochromic windows that control the transmission of light (Rauh, 1999). They form the basis for organic light-emitting diodes (OLEDs) (Armstrong *et al.*, 2001) of the type now used for televisions (van der Vaart *et al.*, 2005). By exploiting the volume change of polymer films during oxidation and reduction, one can use them to create electrochemical actuators (Jager *et al.*, 2000) or artificial muscles (Smela, 2003). One important application of such conjugated polymer devices is their use in electrogenerated chemiluminescence (ECL) (Richter, 2004), a phenomenon that has applications to such areas as fingerprinting (Xu *et al.*, 2012). A robust knowledge of the behaviour of the underlying kinetics is crucial to controlling and optimizing such devices.

One key feature of such systems is a sharp front in the concentration of ionic clusters, which causes bright patterns in ECL experiments (Guo *et al.*, 2011). Since the front propagates with time, these patterns are sometimes referred to as 'ECL waves' or 'ECL solitons' (Chang *et al.*, 2009; Chen *et al.*, 2011). This latter characterization, implying as it does a travelling-wave solution with constant speed, is problematic. While experiments exhibiting sharp fronts in such systems have existed for years (Aoki *et al.*, 1992), some experiments show the front $s(t)$ behaving in a standard Fickian fashion, proportional to $t^{1/2}$ (Tezuka *et al.*, 1999), while others claim to see $s(t) \propto t$ (Tezuka *et al.*, 1991; Wang *et al.*, 2004), and still others see both behaviours, depending on experimental parameters (Wang & Smela, 2009).

Constant front speed is plausible in these systems due to the polymeric nature of the film. As the ionic clusters move into previously 'dry' regions of the polymer, the polymer turns 'wet' (Guo *et al.*, 2011), which induces swelling and other structural changes (Chang *et al.*, 2009). This behaviour is reminiscent of 'Case II' diffusion in polymers (Thomas & Windle, 1982). Including viscoelastic stress effects due to swelling in polymer-penetrant networks can produce fronts which move with constant speed (Edwards, 1995). However, most of the models for ECL systems to date have included only diffusive effects (Lacroix *et al.*, 1998), though several have highly nonlinear diffusion coefficients (Wang *et al.*, 2009). Since Fickian models allow similarity solutions depending on $x/\sqrt{t}$, it is unlikely that such models can capture constant-speed behaviour (Wang *et al.*, 2009).

In Guo *et al.* (2011), the authors present a Fickian-type model which they analyse via numerical simulations. They claim that the simulations demonstrate that the model allows sharp fronts moving with constant speed. We shall examine the same model using an asymptotic approach. We shall show that though the model does indeed allow quite sharp fronts, they move proportional to $t^{1/2}$.

2. Governing equations

2.1 *The full model*

The full description of the model under consideration is provided in Guo *et al.* (2011); below we summarize the relevant details for our purposes. The ECL wave is modelled through the concentration C of ionic clusters through a polymer matrix. The relevant (dimensionless) diffusion equation is the following:

$$\frac{\partial C}{\partial t} = \frac{\partial}{\partial x}\left[D(C)\frac{\partial C}{\partial x}\right], \tag{2.1a}$$

$$D(C) = \frac{D_{\mathrm{w}}}{1+\mathrm{e}^{-\kappa(C-C_{\mathrm{T}})}} + D_{\mathrm{d}}, \tag{2.1b}$$

where the subscripts 'w' and 'd' refer to 'wet' and 'dry'. Here C_{T} is a saturation concentration above which we consider the polymer to be 'wet'. Initially there are no clusters in the polymer, so

$$C(x,0) = 0. \tag{2.2}$$

In Guo *et al.* (2011) the relevant spatial interval is taken as $x \in [-1,1]$; however, the problem they pose is even, so we take the interval as $x \in [0,1]$ with

$$\frac{\partial C}{\partial x}(0,t) = 0. \tag{2.3a}$$

At the other boundary, a constant concentration of clusters is supplied:

$$C(1,t) = 1. \tag{2.3b}$$

2.2 *Asymptotic simplifications*

Such polymers are observed to have great changes in the diffusion coefficient localized about a transition between a conductive and non-conductive state (in our terminology, wet and dry). Hence certain previous models of these systems use a piecewise-constant form for D (Lacroix *et al.*, 1998). Such a form is just the limit of the sigmoidal form (2.1b) for large κ; sharp fronts have been observed in the

solutions to (2.1) when κ is around 30 (Guo *et al.*, 2011). The dramatic behaviour is due to the fact that κ is exponentiated.

Taking $\kappa \to \infty$ in our model yields the following piecewise-constant model, to leading order:

$$D(C) = \begin{cases} D_\mathrm{d}, & C < C_\mathrm{T} \text{ (dry)}, \\ D_\mathrm{w} + D_\mathrm{d}, & C > C_\mathrm{T} \text{ (wet)}, \end{cases} \tag{2.4}$$

as long as $C - C_\mathrm{T} = \mathrm{O}(1)$, that is, away from the moving boundary $s(t)$ where

$$C(s(t), t) = C_\mathrm{T}. \tag{2.5a}$$

Note from the boundary conditions that

$$s(0) = 1. \tag{2.5b}$$

In addition, the diffusion coefficients in the two regions are vastly different; in particular, D_d is taken to be much smaller than D_w (Guo *et al.*, 2011; Lacroix *et al.*, 1998). Hence we rewrite the ratio between them as

$$\frac{D_\mathrm{d}}{D_\mathrm{w}} = \frac{D_*}{\kappa}, \tag{2.6}$$

where D_* is considered to be $\mathrm{O}(1)$.

With (2.4) replacing (2.1b), the original system may be rewritten as a moving boundary-value problem. Using the same subscripts as before, we have the following in the dry region:

$$\frac{\partial C_\mathrm{d}}{\partial t} = D_\mathrm{d} \frac{\partial^2 C_\mathrm{d}}{\partial x^2}, \quad 0 < x < s(t), \tag{2.7a}$$

$$\frac{\partial C_\mathrm{d}}{\partial x}(0, t) = 0, \quad C_\mathrm{d}(x, 0) = 0. \tag{2.7b}$$

Note that this solution exists only until $s(t) = 0$; after that time, the wet solution will occupy the entire domain. The system in the wet region is given by

$$\frac{\partial C_\mathrm{w}}{\partial t} = (D_\mathrm{w} + D_\mathrm{d}) \frac{\partial^2 C_\mathrm{w}}{\partial x^2}, \quad s(t) < x < 1, \tag{2.8a}$$

$$C_\mathrm{w}(1, t) = 1, \tag{2.8b}$$

where there is no initial condition since initially the polymer is dry. To close the system, we use (2.4) in a flux balance across the front to obtain

$$D_\mathrm{d} \frac{\partial C_\mathrm{d}}{\partial x}(s^-(t), t) = (D_\mathrm{w} + D_\mathrm{d}) \frac{\partial C_\mathrm{w}}{\partial x}(s^+(t), t). \tag{2.9}$$

Equations (2.7) and (2.8) form a Stefan-like problem which can be solved for C_w and C_d. We call this solution the *piecewise solution*, as it results from taking $D(C)$ piecewise constant. Note these solutions will not be accurate near $x = s(t)$, where $C \approx C_\mathrm{T}$ and the true sigmoidal behaviour of (2.1b) comes into play. (We eschew the typical perturbation parlance of 'outer solution' because it will be shown that the piecewise solution has an interior layer.)

The flaw can also be seen by noting that the true solution of (2.1) must be continuous, while the piecewise solution will have a jump in $\partial C/\partial x$ by (2.9). To smooth this jump, we will derive a *smoothing*

solution in a corner layer about $(x, C) = (s(t), C_T)$. When deriving these solutions in Sections 3 and 4, we will focus on the leading-order terms only. Corrections will be discussed in Section 5.

3. The piecewise solution

3.1 *The dry region and the similarity variable*

With D_d now $O(\kappa^{-1})$ by (2.6), the leading order of (2.7a) becomes

$$\frac{\partial C_d}{\partial t} = 0. \tag{3.1}$$

Solving (3.1) subject to (2.7b), we have

$$C_d(x, t) = 0, \quad 0 < x < s(t). \tag{3.2}$$

We note that to leading order, the dry solution satisfies (2.3a). Therefore, for time bounded away from t_{max}, where

$$s(t_{max}) = 0, \tag{3.3}$$

the presence of the symmetry boundary does not affect the evolution of the solution. In particular, as long as $t_{max} - t = O(1)$, the solution is the same (to leading order) as if $C_d(x, t) \equiv 0$ for all $x < s(t)$. This formulation is quite analogous to the one-phase Stefan problem (Alexiades & Solomon, 1993, Section 2.1), which has a similarity-variable solution where $s(t) \propto \sqrt{t}$.

Therefore, we introduce the similarity variable

$$\zeta = \frac{1 - x}{2\sqrt{D_w t}} \implies s(t) = 1 - 2\zeta_s \sqrt{D_w t}, \tag{3.4}$$

where ζ_s is a positive constant. (The somewhat non-standard form for $s(t)$ appears because the front moves from right to left in x.) Hence, we have from (3.3) that

$$t_{max} = \frac{1}{4\zeta_s^2 D_w}; \tag{3.5}$$

after that the wet solution occupies the entire domain.

Though our discussion above related to the piecewise solution, since (2.1a) is purely Fickian, the similarity-variable approach will hold for the full solution as well. Therefore, substituting (3.4) into (2.1a), (2.3b) and (2.5a), we obtain

$$\frac{d}{d\zeta}\left(\frac{D(C)}{D_w}\frac{dC}{d\zeta}\right) + 2\zeta\frac{dC}{d\zeta} = 0, \tag{3.6}$$

$$C(0) = 1, \tag{3.7a}$$

$$C(\zeta_s) = C_T. \tag{3.7b}$$

Note that by defining ζ in this way, we shift the Dirichlet condition (3.7a) to the more familiar location $\zeta = 0$.

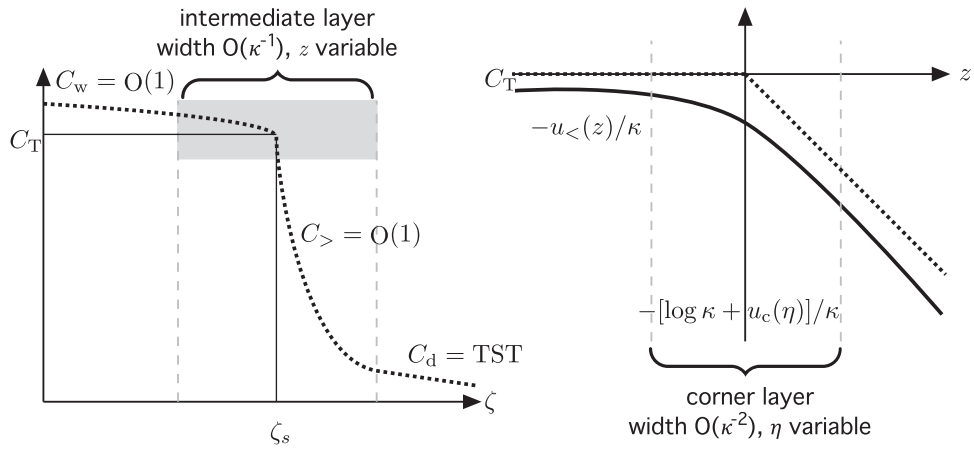

FIG. 1. Left: piecewise solution (dotted). Right: blowup of shaded region illustrating intermediate and corner layers. The dotted curve is the piecewise solution; the solid is the smoothed solution. Variables indicated are the corrections to C_T in the indicated regions.

In order to complete the piecewise solution, we must find the solution in the wet region, which requires the similarity-variable analogue of (2.9):

$$D_d \frac{dC_d}{d\zeta}(\zeta_s^+) = (D_w + D_d)\frac{dC_w}{d\zeta}(\zeta_s^-). \tag{3.8}$$

Note that the $\pm$ superscripts on ζ_s have switched due to the negative sign in the definition of ζ in (3.4).

3.2 *The dry intermediate layer*

Since (3.2) does not satisfy (3.7b), a layer is needed near $x = s(t)$. As several different layers will be needed in the analysis, we illustrate them with a schematic in Fig. 1.

The first internal layer needed is of width $O(\kappa^{-1})$; as it is not the thinnest layer needed, we call it the *intermediate layer*. We let

$$C_d(\zeta) = C_>(z) + o(1), \quad z = \kappa(\zeta - \zeta_s), \tag{3.9}$$

where the subscript '>' refers to the region where $z > 0$, which indicates we are solving only for the dry solution. Since $C - C_T = O(1)$ in this region, we may use the piecewise-constant form for $D(C)$ in (2.4). Substituting (3.9) into (3.6), we have, to leading order,

$$D_* \frac{d^2C_>}{dz^2} + 2\zeta_s \frac{dC_>}{dz} = 0, \quad z > 0, \tag{3.10}$$

where we have used (2.6).

To obtain the boundary conditions on (3.10), we first substitute (3.9) into (3.7b):

$$C_>(0) = C_T. \tag{3.11a}$$

In addition, the boundary-layer solution must match to (3.2) as $\zeta \to \infty$, so we have

$$C_>(\infty) = 0. \tag{3.11b}$$

Solving (3.10) subject to (3.11) yields

$$C_>(z) = C_{\mathrm{T}} \exp\left(-\frac{2\zeta_s z}{D_*}\right). \tag{3.12}$$

3.3 *The wet region*

Substituting (3.12) into (3.8), we obtain, to leading order,

$$\frac{\mathrm{d}C_{\mathrm{w}}}{\mathrm{d}\zeta}(\zeta_s^-) = -2C_{\mathrm{T}}\zeta_s, \tag{3.13}$$

which becomes the new front condition on C_{w} in the piecewise problem. The operator that holds is derived by substituting (2.4) into (3.6), yielding

$$\frac{\mathrm{d}^2 C_{\mathrm{w}}}{\mathrm{d}\zeta^2} + 2\zeta\frac{\mathrm{d}C_{\mathrm{w}}}{\mathrm{d}\zeta} = 0, \quad 0 < \zeta < \zeta_s, \tag{3.14}$$

to leading order. Note the domain on (3.14), which indicates that we are solving only in the wet region. Solving (3.14) subject to (3.7), we have the following:

$$C_{\mathrm{w}}(\zeta) = 1 - (1 - C_{\mathrm{T}})\frac{\operatorname{erf}\zeta}{\operatorname{erf}\zeta_s}. \tag{3.15}$$

Substituting (3.15) into (3.13), we obtain an implicit expression for the value of ζ_s characterizing the front speed:

$$(1 - C_{\mathrm{T}})\mathrm{e}^{-\zeta_s^2} = C_{\mathrm{T}}\zeta_s \operatorname{erf}\zeta_s\sqrt{\pi}. \tag{3.16}$$

Note that (3.16) is independent of D_{w} (since that dependence is scaled away in the definition of ζ). Also note that (3.16) will have a unique solution, since the left-hand side is strictly decreasing from $1 - C_{\mathrm{T}}$ to 0, while the right-hand side is strictly increasing from 0 to ∞. In particular, with the value of C_{T} given in Guo *et al.* (2011), we have that

$$C_{\mathrm{T}} = 0.95 \implies \zeta_s = 0.1608. \tag{3.17a}$$

Then using the value of D_{w} given in Guo *et al.* (2011), we obtain

$$D_{\mathrm{w}} = 0.1 \implies t_{\max} = 96.6552. \tag{3.17b}$$

A graph of the piecewise solution is shown in Fig. 2. As expected, it exhibits a discontinuity in the derivative at $\zeta = \zeta_{\mathrm{s}}$ which must be smoothed.

4. The smoothing solution

The solution in Section 3 is not smooth at the front $\zeta = \zeta_s$ due to the piecewise-constant nature of (2.4) used in its derivation. However, the true solution must be smooth since the true diffusion coefficient

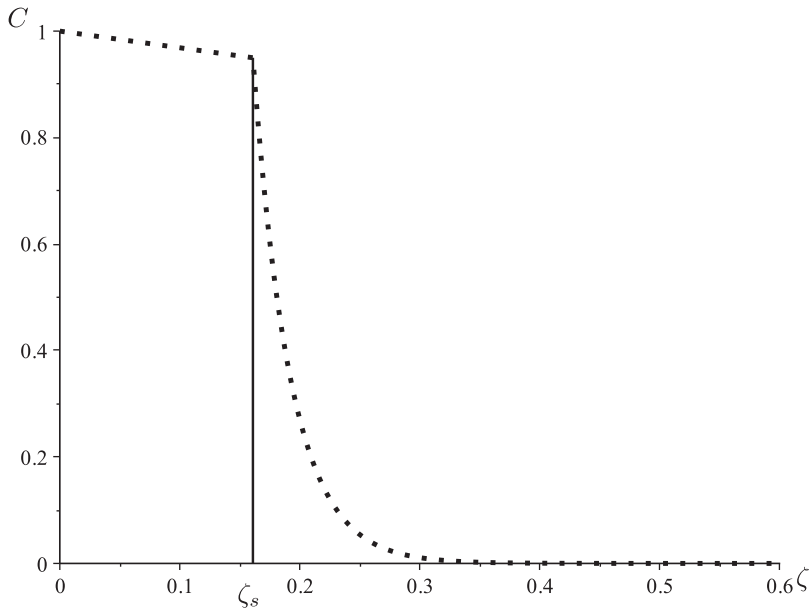

FIG. 2. Piecewise solution with jump in derivative at $\zeta = \zeta_s$.

is given by (2.1b). On the z-scale, the dry solution varies as given by (3.12), while the wet solution is simply C_T to leading order. Hence we must insert a corner layer to smooth the resulting discontinuous derivative. To discern the proper scalings, we substitute (2.1b) and the definition of z in (3.9) into (3.6):

$$\frac{\mathrm{d}}{\mathrm{d}z}\left(\left[\frac{\kappa}{1+\mathrm{e}^{-\kappa(C-C_T)}}+D_*\right]\frac{\mathrm{d}C}{\mathrm{d}z}\right)=-2\zeta_s\frac{\mathrm{d}C}{\mathrm{d}z}. \tag{4.1}$$

We may use (4.1) to obtain physical insights into the system. In the dry region, $C < C_T$, the exponential becomes large, and the D_* term dominates. This forces a balance between the D_* term (representing diffusion in the dry region under the piecewise-constant formulation) and the right-hand side (which is the evolution term $\partial C/\partial t$ term rewritten in the z variables). Hence the z-scale is the diffusion length scale in the dry region [as seen in (3.10)]. In the wet region, $C > C_T$, the exponential becomes small, and the first term on the left-hand side dominates. This causes a constant wet solution in the intermediate layer, reflecting the fact that the z length scale is shorter than the diffusion length scale in the wet region.

4.1 *Matching the corner layer to the dry region*

In the corner layer, we must keep track of the entire structure of $D(C)$ by balancing the two bracketed terms in (4.1). By selecting a scaling that forces the exponential to be $\mathrm{O}(\kappa)$, both bracketed terms are $\mathrm{O}(1)$. Therefore, we introduce the following substitution, whose non-standard form is motivated by the structure of (2.1b):

$$C_c(z)=C_T-\frac{\log\kappa}{\kappa}-\frac{u_c(\eta)}{\kappa}+o(\kappa^{-1}),\quad \eta=\kappa z, \tag{4.2}$$

where the subscript 'c' denotes 'corner'. The proper width of the corner layer has been derived by matching the derivatives as we exit the corner layer to the right:

$$\frac{\mathrm{d}C_>}{\mathrm{d}z}(0^+) = -\frac{\kappa}{\kappa}\frac{\mathrm{d}u_\mathrm{c}}{\mathrm{d}\eta}(\infty) \quad \Longrightarrow \quad \frac{\mathrm{d}u_\mathrm{c}}{\mathrm{d}\eta}(\infty) = \frac{2C_\mathrm{T}\zeta_s}{D_*}, \tag{4.3}$$

where we have used (3.12). The reason for the addition of the constant term between C_T and u_c becomes clear when we substitute (4.2) into (4.1). The leading order of the result is

$$\frac{\mathrm{d}}{\mathrm{d}\eta}\left(\left[\frac{\kappa}{1+\kappa \mathrm{e}^{u_\mathrm{c}}} + D_*\right]\frac{\mathrm{d}u_\mathrm{c}}{\mathrm{d}\eta}\right) = 0. \tag{4.4}$$

Hence this term forces a balance between the two bracketed terms as $\kappa \to \infty$.

Integrating (4.4) with respect to ζ, we have, to leading order,

$$\left(\frac{1}{\mathrm{e}^{u_\mathrm{c}}} + D_*\right)\frac{\mathrm{d}u_\mathrm{c}}{\mathrm{d}\eta} = 2\zeta_s C_\mathrm{T}, \tag{4.5}$$

where we have used (4.3). Since the left-hand side is just the flux, (4.5) says that the flux is constant throughout the corner layer. (Recall that a constant flux led to a discontinuous derivative in the piecewise solution because the diffusion coefficient was discontinuous.) Integrating (4.5) again, we obtain

$$D_* u_\mathrm{c} - \mathrm{e}^{-u_\mathrm{c}} = 2\zeta_s C_\mathrm{T}\eta + A, \tag{4.6}$$

which defines an implicit relation for u_c. Here A is a constant yet to be determined.

There is a discrepancy when trying to match (4.2) and (3.12) as $\eta \to \infty$. In particular, we note that the proper balance in (4.6) as $\eta \to \infty$ is between the first terms on each side. Thus we may rewrite (4.2) in the matching limit as

$$\begin{aligned} C_\mathrm{c}(\eta) &\sim C_\mathrm{T} - \frac{\log\kappa}{\kappa} - \frac{2\zeta_s C_\mathrm{T}\eta}{\kappa D_*} - \frac{A}{\kappa D_*}, \quad \eta \to \infty, \\ C_\mathrm{c}(z) &\sim C_\mathrm{T}\left(1 - \frac{2\zeta_s z}{D_*}\right) - \frac{\log\kappa}{\kappa} - \frac{A}{\kappa D_*}, \quad z \to 0^+. \end{aligned} \tag{4.7}$$

The first two terms in (4.7) match the first two terms in the expansion of (3.12) for small z. The third term does not match, but indicates what the size in the next term of the expansion for $C_>$ should be. Note that the contribution from A is even smaller.

We conclude by writing the uniformly valid solution in the dry region:

$$C(\zeta) = C_\mathrm{T}\left[\exp\left(-\frac{2\zeta_s\kappa(\zeta-\zeta_s)}{D_*}\right) + \frac{2\zeta_s\kappa(\zeta-\zeta_s)}{D_*}\right] - \frac{\log\kappa}{\kappa} - \frac{u_\mathrm{c}(\eta)}{\kappa}, \quad \zeta > \zeta_s. \tag{4.8}$$

Note that the domain restriction on ζ still holds, since the solution contains the exponential term which diverges for $\zeta < \zeta_s$.

4.2 *The wet intermediate layer*

To construct the uniform solution in the wet region, we examine the behaviour of u_c as $\eta \to -\infty$, which should then match to C_w. As $\eta \to -\infty$, the exponential on the left-hand side of (4.6) dominates, so

we have

$$u_c \sim -\log(2\zeta_s C_T|\eta| - A), \quad \eta \to -\infty,$$
$$C_c(z) \sim C_T + \frac{1}{\kappa}\left[\log(2\zeta_s C_T|z|) - \frac{A}{2\kappa\zeta_s C_T|z|}\right], \quad z \to 0^-. \tag{4.9}$$

Since the logarithmic behaviour does not match the outer solution C_w, there must be an intermediate z-layer in the wet region as well. Thus we let

$$C_<(z) = C_T - \frac{u_<(z)}{\kappa} + o(\kappa^{-1}), \tag{4.10}$$

where the subscript '$<$' refers to the domain $z < 0$. Substituting (4.10) into (4.1), we obtain, to leading order,

$$\frac{d}{dz}\left(\frac{\kappa}{1+e^{u_<}}\frac{du_<}{dz}\right) = 0. \tag{4.11}$$

Therefore, in this intermediate region the nonlinear part of the diffusion coefficient is not constant (as it is for ζ away from ζ_s), but it is not so small that the D_* term comes into play (as it does in the η region).

Solving (4.11) subject to the matching condition in (4.9) (rewritten in the $u_<$ variable), we have

$$u_<(z) = -2\zeta_s C_T|z| - \log(1 - e^{-2\zeta_s C_T|z|}),$$
$$C_<(\zeta) = C_T - 2\zeta_s C_T(\zeta - \zeta_s) + \frac{1}{\kappa}\log(1 - e^{-2\kappa\zeta_s C_T(\zeta_s - \zeta)}). \tag{4.12}$$

In order to match $C_<$ to C_w, we expand the latter [as given in (3.15)] for ζ near ζ_s:

$$C_w(\zeta) \sim C_T - 2C_T\zeta_s(\zeta - \zeta_s), \quad \zeta \to \zeta_s^-. \tag{4.13}$$

The first two terms of (4.12) match (4.13); hence the uniform solution for these two regions is given by

$$C(\zeta) = 1 - (1 - C_T)\frac{\operatorname{erf}\zeta}{\operatorname{erf}\zeta_s} + \frac{1}{\kappa}\log(1 - e^{-2\kappa\zeta_s C_T(\zeta_s - \zeta)}). \tag{4.14}$$

4.3 *Matching the wet intermediate layer to the corner layer*

Equation (4.14) is good for ζ away from ζ_s. To construct the uniform solution, we must find the common part that arises when we match this to the corner-layer solution. As $\zeta \to \zeta_s^-$, the argument of the logarithm tends to zero, which exactly matches the behaviour described in (4.9). Rewriting the leading order of (4.9) in terms of the outer variable, we have

$$C_c(\zeta) \sim C_T + \frac{1}{\kappa}\log(2\zeta_s C_T\kappa(\zeta_s - \zeta)), \quad \zeta \to \zeta_s^-, \tag{4.15}$$

which forms the common part. (Note that again the A contribution is subdominant.)

Hence the uniform solution for negative $\zeta < \zeta_s$ is given by

$$C(\zeta) = 1 - (1 - C_{\mathrm{T}})\frac{\operatorname{erf}\zeta}{\operatorname{erf}\zeta_s} + \frac{1}{\kappa}\log\left(\frac{1 - \mathrm{e}^{-2\kappa\zeta_s C_{\mathrm{T}}(\zeta_s - \zeta)}}{2\kappa\zeta_s C_{\mathrm{T}}(\zeta_s - \zeta)}\right) - \frac{\log\kappa}{\kappa} - \frac{u_{\mathrm{c}}(\eta)}{\kappa}, \quad \zeta < \zeta_s. \tag{4.16}$$

As $\zeta \to \zeta_s^-$, the argument of the logarithm in (4.16) goes to 1, so the blowup inherent in (4.14) no longer occurs. For ζ away from ζ_s, the logarithm term gets large, but is multiplied by the κ^{-1} term, eventually producing another term of $\mathrm{O}((\log\kappa)/\kappa)$.

5. Solution analysis

5.1 *Discussion of correction terms*

To plot the solution, we need the parameter values in (3.17a). Motivated by the calculations in Guo *et al.* (2011), we choose $\kappa = 100$. Note that with such a definition of κ, one could argue that $C - C_{\mathrm{T}} = o(1)$ throughout the wet region. However, as we can solve the problem without this assumption, we do not impose it.

To determine the importance of the parameter A, we note from (4.9) that the term including A (which is the one not included in the matching) is $\mathrm{O}(\kappa^{-2})$ in the wet region. However, the error we make by approximating $D(C)/D_{\mathrm{w}}$ in (3.6) by 1 in (3.14) is $\mathrm{O}(\kappa^{-1})$. Hence the expansion for the solution in the wet region would be of the form:

$$C_{\mathrm{w}}(\zeta) = 1 - (1 - C_{\mathrm{T}})\frac{\operatorname{erf}\zeta}{\operatorname{erf}\zeta_s} + \kappa^{-1}u_{\mathrm{w}}(\zeta) + o(\kappa^{-1}), \tag{5.1}$$

and the contribution from the A term is subdominant. Also from (4.7), we have that the term including A is $\mathrm{O}(\kappa^{-1})$ in the dry region. Hence to get just the leading-order solution, we may take $A = 0$. The graph is shown in Fig. 3, which illustrates the solution for various values of D_*.

The graph looks physical in the wet region, and it can be shown that $C(0) \approx 1 - 2\kappa^{-2}$, as would be expected by ignoring the contribution from A. However, the graph goes negative in the dry region. The reason can be seen from (4.7), where the largest unmatched term is $-(\log\kappa)/\kappa$. Hence in the dry intermediate layer, the proper expansion is

$$C(z) = C_{\mathrm{T}}\exp\left(-\frac{2\zeta_s z}{D_*}\right) + \frac{\log\kappa}{\kappa}u_{>}(z) + o\left(\frac{\log\kappa}{\kappa}\right), \quad z > 0. \tag{5.2}$$

As long as C is bounded away from C_{T}, the operator in (2.7a) holds at all orders (in other words, C_{d} is transcendentally small). Hence we have that

$$u_{>}(\infty) = 0. \tag{5.3a}$$

At the corner layer, $u_{>}$ must match with the currently unmatched $-(\log\kappa)/\kappa$ term, so we have

$$u_{>}(0) = -1. \tag{5.3b}$$

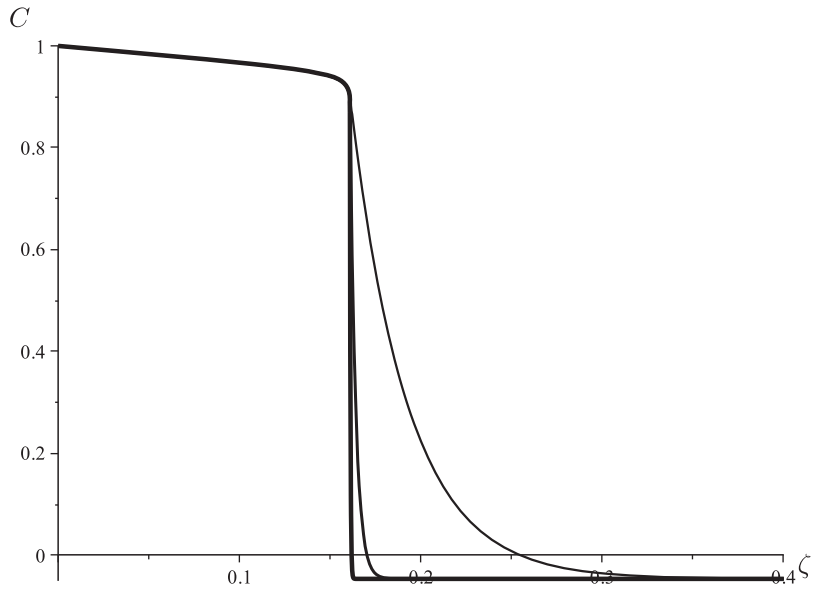

FIG. 3. Leading-order uniform similarity solution *vs.* ζ for Cartesian case. In increasing order of thickness: $D_* = 1, 0.1, 0.01$.

As long as C is bounded away from C_T, the operator in (3.10) holds at all orders. Hence the solution for $u_>(z)$ is exactly analogous to (3.12), the solution in the dry intermediate layer is now given by

$$C(z) = \left(C_\mathrm{T} - \frac{\log\kappa}{\kappa}\right)\exp\left(-\frac{2\zeta_s z}{D_*}\right), \quad z > 0,$$

and the uniformly valid solution analogous to (4.8) is

$$C(\zeta) = C_\mathrm{T}\left[\exp\left(-\frac{2\zeta_s\kappa(\zeta-\zeta_s)}{D_*}\right) + \frac{2\zeta_s\kappa(\zeta-\zeta_s)}{D_*}\right] - \frac{\log\kappa}{\kappa}\exp\left(-\frac{2\zeta_s z}{D_*}\right) - \frac{u_\mathrm{c}(\eta)}{\kappa}, \quad \zeta > \zeta_s. \tag{5.3c}$$

The graph including $u_>(z)$ is shown in Fig. 4; note that the solution remains positive and smooth, as desired. As D_* increases, the diffusion coefficient in the dry region becomes larger. This causes the profile to decay over a larger region, as more diffusion takes place in the dry intermediate layer. For $D_* = 1$, there is a 'shoulder-like' profile to the graph, as the very sharp bend in the curve in the corner layer connects to a much wider profile in the dry region. This profile is indicative of experimental data for these systems (Tezuka *et al.*, 1991, 1999; Wang *et al.*, 2004; Wang & Smela, 2009).

5.2 *Comparison with numerics*

In order to validate our asymptotic solution, we match it to numerical simulations using the algorithm in Edwards (2013). Here as in Edwards (2013) we take $D_* = 0.01$ in order to compare with the results in Guo *et al.* (2011). The results are shown in Fig. 5. Note that the front progresses from right to left (recall

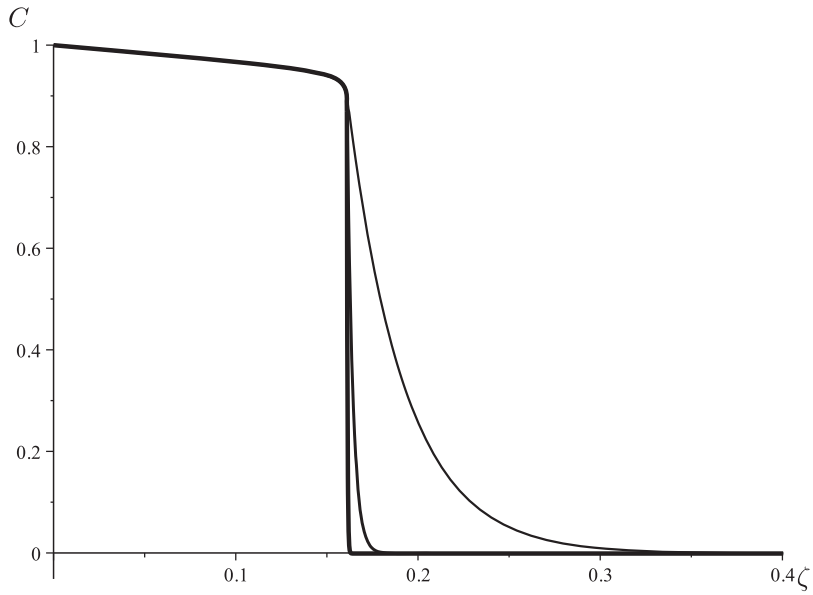

FIG. 4. Uniform similarity solution vs ζ for Cartesian case, including $u_>$. In increasing order of thickness: $D_* = 1, 0.1, 0.01$.

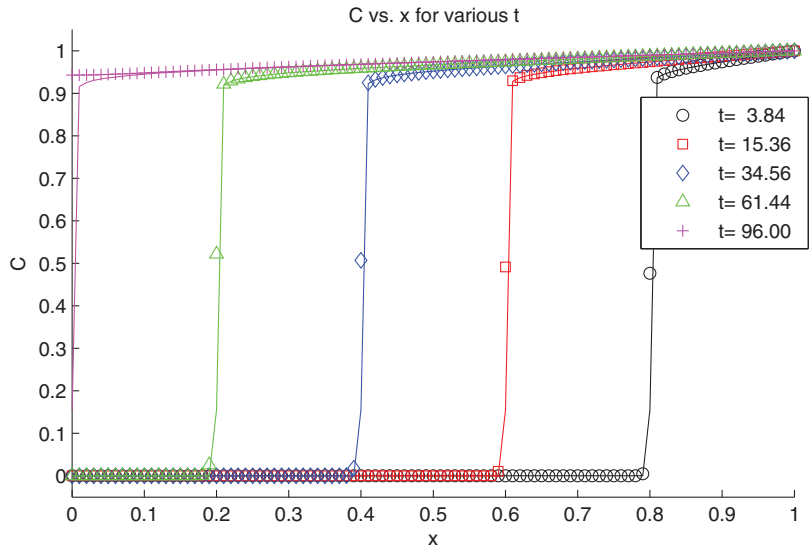

FIG. 5. Numerical (symbol) and asymptotic (line) concentration profiles for $D_* = 0.01$.

that ζ is oriented opposite to x). Given the $\sqrt{t}$ behaviour of s, the time intervals have been chosen so that the front moves a fixed amount between curves. Note the close agreement between the numerical and asymptotic solutions, with significant differences visible only for the last time snapshot. (Recall from (3.17b) that $t_{\max} = 96.6552$.) As the main case of experimental interest is the progression of the wet/dry

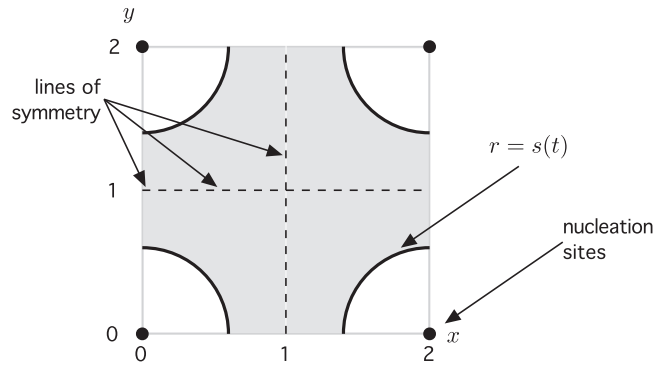

FIG. 6. Repeating cell from experimental setup. Concentration is zero to leading order in shaded areas.

interface through the bulk of the domain, we relegate a discussion of what happens for t near and greater than $t_{\max}$ to the appendix.

Though the asymptotic solutions used in Edwards (2013) and this manuscript are different, Fig. 5 shows a striking similarity to Fig. 4 in Edwards (2013). The similarity may be explained by noting that in that paper, the author ignored the $u_>(z)$ term, but chose A to match the numerical and asymptotic solutions at the first time step, which essentially forced $C(\infty) = 0$. Thus the matching term $-A/\kappa D_*$ from (4.7) must equal $(\log \kappa)/\kappa$ so that the far-field asymptotic solution would be zero. Setting these two terms equal and using the given numerical parameters, we have

$$A = -D_* \log \kappa = -0.0461. \tag{5.4}$$

This is actually the value of A found by the author in Edwards (2013); the value quoted in the paper has a typographical error.

6. Polar coordinates

In the real experimental system, the ionic clusters diffuse from a square array of copper posts; these are called ECL 'nucleation sites' or 'triggers' in the literature (Guo *et al.*, 2011). This produces a series of repeating cells with point sources at the corners (see Fig. 6). Hence the Cartesian model postulated in Guo *et al.* (2011) and analysed above is a representation of a one-dimensional slice of the polymer (for instance, at $y = 0$ in Fig. 6). We conclude by presenting some preliminary results on the full system in polar coordinates. For simplicity, we focus on deriving uniformly valid solutions for the time when the wet and dry polymer stages coexist.

6.1 *Governing equations*

Owing to the nature of the repeating cell, all the boundaries of the square shown in Fig. 6 are lines of symmetry, as are the dashed lines. The form of $D(C)$ may still initially be taken piecewise constant as in (2.4). Moreover, with D_{d} still taken to be small, equation (3.1) still holds. Hence in the dry region (shaded in Fig. 6), the leading-order concentration remains zero, and a similarity approach may work.

Hence we introduce polar coordinates with the origin centred at the source in the lower-left corner of the square, so the waves move from left to right in this formulation. There is no angular dependence in the problem until the time at which the expanding disks coalesce. Consideration of this interval is beyond the scope of this manuscript. Hence we may rewrite the concentration as $C(r,t)$, leading to the following equation which replaces (2.1a):

$$\frac{\partial C}{\partial t} = \frac{1}{r}\frac{\partial}{\partial r}\left[D(C) r \frac{\partial C}{\partial r}\right], \quad r > r_0, \tag{6.1}$$

where r_0 is the radius of the posts.

6.2 *The piecewise solution*

In the limit that $\kappa \to \infty$, diffusion of C_d is given by

$$\frac{\partial C_\mathrm{d}}{\partial t} = \frac{D_\mathrm{d}}{r}\frac{\partial}{\partial r}\left(r\frac{\partial C_\mathrm{d}}{\partial r}\right), \quad r > s(t). \tag{6.2}$$

Since $D_\mathrm{d} \to 0$, (3.1) still holds for C_d. Hence so does (3.2), rewritten in the proper variables:

$$C_\mathrm{d}(r,t) = 0, \quad r > s(t). \tag{6.3}$$

As before, this solution motivates a similarity-variable approach. Therefore, we let

$$\zeta = \frac{r - r_0}{2\sqrt{D_\mathrm{w} t}} \implies s(t) = r_0 + 2\zeta_s\sqrt{D_\mathrm{w} t}. \tag{6.4}$$

Substituting (6.4) into the full equation (6.1) as well as the boundary condition (2.9), we have

$$\frac{\mathrm{d}}{\mathrm{d}\zeta}\left(\zeta\frac{D(C)}{D_\mathrm{w}}\frac{\mathrm{d}C}{\mathrm{d}\zeta}\right) + 2\zeta^2\frac{\mathrm{d}C}{\mathrm{d}\zeta} = 0, \quad 0 < \zeta < \zeta_s, \tag{6.5}$$

$$D_\mathrm{d}\frac{\mathrm{d}C_\mathrm{d}}{\mathrm{d}\zeta}(\zeta_s^+) = (D_\mathrm{w} + D_\mathrm{d})\frac{\mathrm{d}C_\mathrm{w}}{\mathrm{d}\zeta}(\zeta_s^-). \tag{6.6}$$

Note that (6.6) is of the same form as (3.8). In addition, (3.7b) still holds.

We cannot solve the problem in the wet region without a proper flux condition in the front, which requires solving in the dry intermediate layer. To do so, we again introduce the variables in (3.9). Making these substitutions into (6.5), we obtain (3.10) to leading order. When introducing a layer very near a surface, its curvature can be ignored, and hence the polar and Cartesian intermediate-layer equations are identical. As the matching conditions are the same as before, the solution for $C_>$ is again given by (3.12). With the solution thus determined, the flux condition (6.6) [which is the same as (3.8)] becomes (3.13).

In the wet region, (6.5) becomes

$$\frac{\mathrm{d}}{\mathrm{d}\zeta}\left(\zeta \mathrm{e}^{\zeta^2}\frac{\mathrm{d}C_\mathrm{w}}{\mathrm{d}\zeta}\right) = 0,$$

which has solutions

$$C_\mathrm{w}(\zeta) = \frac{AE_1(\zeta^2)}{2} + B, \quad E_1(\zeta^2) = \int_{\zeta^2}^{\infty}\frac{\mathrm{e}^{-y}}{y}\,\mathrm{d}y. \tag{6.7}$$

Here E_1 is the exponential integral, which blows up logarithmically as $\zeta \to 0$ (see Abramowitz & Stegun, 1972, Section 5). Hence a Dirichlet condition $C_w(0) = 1$ as posited in the Cartesian case will lead to the non-physical similarity-variable solution $C_w = 1$ everywhere, and no boundary layer can be inserted.

This is because as t gets larger, the source most propagate a similarity solution over a larger and larger area. The two-dimensional analogue of the one-dimensional Cartesian case has a line of sources fixed at $C = 1$, while in our case we have only a point. Thus, we now posit that the electrode provides a steady source $2\pi Q$ over time. Hence we have that, to leading order

$$\frac{\mathrm{d}}{\mathrm{d}t}\int_0^{2\pi}\int_{r_0}^{\infty} rC(r,t)\,\mathrm{d}r\,\mathrm{d}\theta = 2\pi Q \implies r_0\frac{\partial C_w}{\partial r}(r_0,t) = -\frac{Q}{D_w},$$
$$\frac{\mathrm{d}C_w}{\mathrm{d}\zeta}(0) = -\frac{Q}{D_w r_0},$$

where we have used (6.1) and the fact that there is no flux at infinity. However, the right-hand side above is finite for any non-zero r_0, while the exponential integral has an infinite derivative at $\zeta = 0$. Hence the only way to admit a similarity-variable solution is to take $r_0 \to 0$ and make the post a point source. With proper normalization, the condition there becomes

$$\lim_{r\to 0} r\frac{\partial C_w}{\partial r} = -1. \tag{6.8}$$

Then using (3.7b) and (6.8) to find the constants in (6.7), we obtain

$$C_w(\zeta) = C_T + \frac{E_1(\zeta^2) - E_1(\zeta_s^2)}{2}. \tag{6.9}$$

Obviously the logarithmic singularity in (6.9) is a weakness of the similarity-variable approach to this problem. Possible ways to remedy this weakness are discussed in Section 7.

Substituting (6.9) into (3.13) (which we have established also holds in polar coordinates), we obtain an equation for the front parameter ζ_s:

$$\mathrm{e}^{-\zeta_s^2} = 2C_T\zeta_s^2. \tag{6.10}$$

Note that (6.10) is independent of D_w (since that dependence is scaled away in the definition of ζ). Also note that it will have a unique solution, since the left-hand side is strictly decreasing from 1 to 0, while the right-hand side is strictly increasing from 0 to ∞. In particular, with the value of the physical parameters given in (3.17), we have

$$\zeta_s = 0.604, \quad t_{\max} = 6.8443. \tag{6.11}$$

6.3 *The smoothing solution*

To smooth the solution in the dry region, we write the full equation (6.5) in the z variable, yielding

$$\kappa\frac{\mathrm{d}}{\mathrm{d}z}\left(\kappa\zeta_s\left(\frac{1}{1+\mathrm{e}^{-\kappa(C-C_T)}} + \frac{D_d}{D_w}\right)\frac{\mathrm{d}C}{\mathrm{d}z}\right) + 2\kappa\zeta_s^2\frac{\mathrm{d}C}{\mathrm{d}z} = 0,$$

which reduces to (4.1). Hence the same η-scalings work and lead to the same solution, namely (4.7) [and hence (4.8)]. Moreover, since (4.1) still holds, the smoothing in the wet region proceeds as in the Cartesian case. (Recall that this is because the behaviour of the wet solution must be the same as in

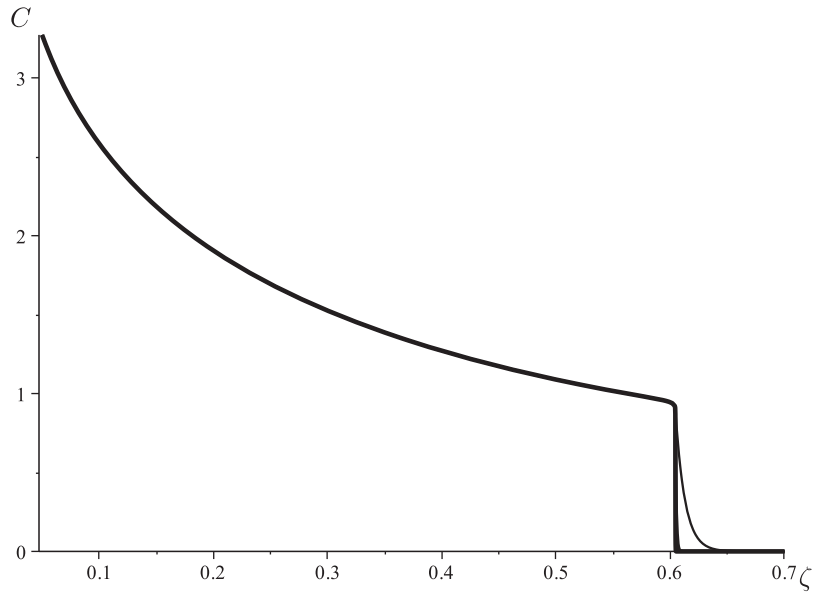

FIG. 7. Uniform similarity solution vs ζ for polar case including $u_>$. In an increasing order of thickness: $D_* = 1$, 0.1, 0.01. ($D_* = 0.1$ case obscured by scale.)

the Cartesian case since the front conditions, which are determined by the dry solution, are the same.) Hence (4.12) still holds, and the uniform solution for the dry and intermediate-layer regions is given by

$$C(\zeta) = C_{\mathrm{T}} + \frac{E_1(\zeta^2) - E_1(\zeta_s^2)}{2} + \frac{1}{\kappa}\log(1 - \mathrm{e}^{-2\kappa\zeta_s C_{\mathrm{T}}(\zeta_s - \zeta)}), \tag{6.12}$$

which replaces (4.14). The remainder of the matching to the corner layer is the same, and hence the final uniform solution for $\zeta < \zeta_s$ is given by

$$C(\zeta) = C_{\mathrm{T}} + \frac{E_1(\zeta^2) - E_1(\zeta_s^2)}{2} + \frac{1}{\kappa}\log\left(\frac{1 - \mathrm{e}^{-2\kappa\zeta_s C_{\mathrm{T}}(\zeta_s - \zeta)}}{2\kappa\zeta_s C_{\mathrm{T}}(\zeta_s - \zeta)}\right) - \frac{\log\kappa}{\kappa} - \frac{u_{\mathrm{c}}(\eta)}{\kappa}, \quad \zeta < \zeta_s. \tag{6.13}$$

In Fig. 7, we plot the radial similarity solution using the same parameters as in Section 5. Owing to the logarithmic blowup of the solution required to keep the flux constant, the ζ-axis is truncated away from $\zeta = 0$. However, even in this graph C increases far past the maximum value of $C = 1$ in the Cartesian case.

7. Conclusions and further research

Scientists would like to understand and predict the phenomenon of electrogenerated chemiluminescence better. This is especially important since experimental data have shown regimes where the propagating ECL wave moves like both t and $t^{1/2}$ (Tezuka *et al.*, 1991; Wang *et al.*, 2004; Wang & Smela, 2009). A more detailed understanding of the dynamics should determine whether the discrepancy is due to experimental noise or due to the underlying polymeric structure of the films. Though diffusion in polymers

can exhibit sharp fronts moving with constant speed (Thomas & Windle, 1982), other effects, such as viscoelastic memory effects, must be incorporated into the model (Edwards, 1995).

In Guo *et al.* (2011), the authors propose a nonlinear Fickian-type model for ECL waves, and claim that their simulations show the model allows for constant front speed. In this work, we examined the model asymptotically and demonstrated that though the nonlinear diffusion coefficient does produce sharp fronts, those fronts still move proportional to $t^{1/2}$. We find the numerical results in Guo *et al.* (2011) suspect, as their front speed decreases inversely with the step size Δx of their simulations.

Because diffusion in the dry region of the polymer is essentially negligible, the operator in the outer region can be posed in the style of a one-phase Stefan problem. Hence a similarity-variable approach can be used, guaranteeing the $t^{1/2}$ front behaviour. In the limit of large κ, four regimes of interest were identified.

There is an intermediate layer of width $O(\kappa^{-1})$ in the dry region which links the front value C_T to the outer dry solution $C_d = 0$. This layer then causes an $O(1)$ balance in the flux, which provides enough conditions on the operator in the outer wet region to close the system. The solution in the outer wet region is a standard error-function profile.

The combination of these two solutions has a discontinuous derivative at the front, which occurs because the diffusion coefficient had been taken to be piecewise constant. Considering the full structure of $D(C)$ in (2.1b) leads to a corner layer of width $O(\kappa^{-2})$ about the front to smooth the solution. The corner-layer solution blows up logarithmically as it enters the wet region. Hence an intermediate layer is also needed in the wet region to match the corner-layer solution to the outer wet solution. The full uniform solution profile matches numerical (Edwards, 2013) and experimental results (Tezuka *et al.*, 1991, 1999; Wang *et al.*, 2004; Wang & Smela, 2009).

The true experimental setup has a series of posts (point sources) in a square array. This motivates a polar-coordinate approach, at least until the time at which the ELC waves coalesce. Moving to polar coordinates requires a modification of the nucleation condition. Since the governing operator in the layer is independent of curvature, all of the layer solutions are the same for both the Cartesian and polar coordinate systems. It is only the wet solution which is different, and it can be represented in terms of the exponential integral.

The similarity solution thus derived, though providing useful results away from the posts, blows up logarithmically at the origin. One way to remedy this defect would be to restate the problem as a singular boundary-value problem (cf. Kevorkian & Cole, 1996, Section 3.3) with conditions given at $r = O(\kappa^{-1})$, and meld this solution to the similarity-variable approach.

It should be emphasized that the results in this manuscript do not rule out constant front speed in ELC polymer systems. Rather, the model in Guo *et al.* (2011) cannot capture such behaviour, and more complicated models including effects such as viscoelasticity would be necessary.

References

Abramowitz, M. & Stegun, I. A. eds. (1972). *Handbook of Mathematical Functions*. Applied Mathematics Series, vol. 155. Washington: U. S. Department of Commerce.

Adhikari, B. & Majumdar, S. (2004). Polymers in sensor applications. *Progr. Polym. Sci.*, **29**, 699–766.

Alexiades, V. & Solomon, A. D. (1993). *Mathematical Modeling of Melting and Freezing Processes*, Hemisphere, Washington.

Aoki, K., Aramoto, T. & Hoshino, Y. (1992). Photographic measurements of propagation speeds of the conducting zone in polyaniline films during electrochemical switching. *J. Electroanal. Chem.*, **340**, 127–135.

Armstrong, N., Wightman, R. & Gross, E. (2001). Light-emitting electrochemical processes. *Annu. Rev. Phys. Chem.*, **52**, 391–422.

Barford, W. (2005). *Electronic and Optical Properties of Conjugated Polymers*. International Series of Monographs on Physics, vol. 129. Oxford: Oxford University Press.

Carrier, G. F. & Pearson, C. E. (1988). *Partial Differential Equations: Theory and Technique*. New York: Academic Press.

Chang, Y.-L., Palacios, R. E., Chen, J.-T., Stevenson, K. J., Guo, S., Lackowski, W. M. & Barbara, P. F. (2009). Electrogenerated chemiluminescence of soliton waves in conjugated polymers. *J. ACS*, **131**, 14166–14167.

Chen, J.-T., Chang, Y.-L., Guo, S., Fabian, O., Lackowski, W. M. & Barbara, P. F. (2011). Electrogenerated chemiluminescence of pure polymer films and polymer blends. *Macromol. Rapid Commun.*, **32**, 598–603.

Edwards, D. A. (1995). Constant front speed in weakly diffusive non-Fickian systems. *SIAM J. Appl. Math.*, **55**, 1039–1058.

Edwards, D. A. (2013). Sharp Fickian behavior of electrogenerated chemiluminescence waves in conjugated polymer films. *J. Phys. Chem. C*, **117**, 6747–6751.

Guo, S., Fabian, O., Chang, Y.-L., Chen, J.-T., Lackowski, W. M. & Barbara, P. F. (2011). Electrogenerated chemiluminescence of conjugated polymer films from patterned electrodes. *J. ACS*, **133**, 11994–12000.

Jager, E., Smela, E. & Inganas, O. (2000). Microfabricating conjugated polymer actuators. *Science*, **290**, 1540–1545.

Kevorkian, J. & Cole, J. D. (1996). *Multiple Scale and Singular Perturbation Methods*. Applied Mathematics Series, vol. 114. Berlin: Springer.

Lacroix, J., Fraoua, K. & Lacaze, P. (1998). Moving front phenomena in the switching of conductive polymers. *J. Electroanal. Chem.*, **444**, 83–93.

Rauh, R. (1999). Electrochromic windows: an overview. *Electrochim. Acta*, **44**, 3165–3176, 3rd International Meeting on Electrochromics (IME-3), Imperial College, London, September 7–9, 1998.

Richter, M. (2004). Electrochemiluminescence (ECL). *Chem. Rev.* **104**, 3003–3036.

Smela, E. (2003). Conjugated polymer actuators for biomedical applications. *Adv. Mat.*, **15**, 481–494.

Tezuka, Y., Aoki, K. & Ishii, A. (1999). Alternation of conducting zone from propagation-control to diffusion-control at polythiophene films by solvent substitution. *Electrochim. Acta*, **44**, 1871–1877, Workshop on the Electrochemistry of Electroactive Polymer Films (WEEPF97), Dourdan, France, September 22–24, 1997.

Tezuka, Y., Ohyama, S., Ishii, T. & Aoki, K. (1991). Observation of propagation speed of conductive front in electrochemical doping process of polypyrrole films. *Bull. Chem. Soc. Japan*, **64**, 2045–2051.

Thomas, N. & Windle, A. (1982). A theory of case II diffusion. *Polymer*, **23**, 529–542.

van der Vaart, N., Lifka, H., Budzelaar, F., Rubingh, J., Hoppenbrouwers, J., Dijksman, J., Verbeek, R., van Woudenberg, R., Vossen, F., Hiddink, M., Rosink, J., Bernards, T., Giraldo, A., Young, N., Fish, D., Childs, M., Steer, W., Lee, D. & George, D. (2005). Towards large-area full-color active-matrix printed polymer OLED television. *J. Soc. Info. Disp.*, **13**, 9–16, International Symposium of the Society for Information Display (SID 2004), Seattle, WA, May 25–27, 2004.

Wang, X., Shapiro, B. & Smela, E. (2004). Visualizing ion currents in conjugated polymers. *Adv. Mat.*, **16**, 1605–1609.

Wang, X., Shapiro, B. & Smela, E. (2009). Development of a model for charge transport in conjugated polymers. *J. Phys. Chem. C*, **113**, 382–401.

Wang, X. & Smela, E. (2009). Experimental studies of ion transport in PPy(DBS). *J. Phys. Chem. C*, **113**, 369–381.

Xu, L., Li, Y., Wu, S., Liu, X. & Su, B. (2012). Imaging latent fingerprints by electrochemiluminescence. *Angew. Chem. Intl. Ed.*, **51**, 8068–8072.

Appendix A. Wet-only solution in Cartesian geometry

For completeness, we discuss what happens in the Cartesian geometry near and after $t_{\max}$. As shown in Fig. 5, as $t \to t_{\max}^-$, the front approaches $x = 0$, and the similarity solution does not satisfy the boundary condition there. Hence a boundary layer near $x = 0$ would need to be inserted for t near $t_{\max}^-$. Such a

boundary-layer expansion is beyond the scope of this manuscript, as the main case of experimental interest is the progression of the wet/dry interface through the bulk of the domain.

Note that the boundary layer would be only in the derivative, and hence in the outer region away from zero we have that

$$C(x, t_{\max}) = 1 - (1 - C_{\mathrm{T}}) \frac{\operatorname{erf} \zeta_s (1 - x)}{\operatorname{erf} \zeta_s}, \tag{A.1}$$

where we have used (3.3).

To construct the solution in the wet-only region where $t > t_{\max}$, we introduce the variable substitution $\tau = t - t_{\max}$. The operator for C is invariant under translation, so (2.8) holds on the entire domain $0 < x < 1$. Since the entire polymer is wet, (2.3a) now applies. The initial condition for the problem is given by (A.1), which holds at $\tau = 0$.

Using standard Fourier series techniques, we may write the leading-order solution as

$$C_{\mathrm{w}}(x, \tau) = 1 - \sum_{n=0}^{\infty} \phi_n \exp\left(-D_{\mathrm{w}} \lambda_n^2 \tau\right) \cos \lambda_n x, \quad \lambda_n = \frac{(2n+1)\pi}{2}, \tag{A.2}$$

where we have used the fact that $D_{\mathrm{d}} \ll 1$. Hence any boundary layer in the derivative near $x = 0$ for $t < t_{\max}$ will become moot for $t > t_{\max}$ and the purely diffusive operator applies.

The ϕ_n are given by the initial conditions:

$$\phi_n = \frac{2(1 - C_{\mathrm{T}})}{\operatorname{erf} \zeta_s} \int_0^1 \operatorname{erf} \zeta_s (1 - x) \cos(\lambda_n x)\, \mathrm{d}x.$$

After some tedious manipulations, we find that

$$\phi_n = \frac{4 C_{\mathrm{T}} \zeta_s}{\lambda_n} \Re[\mathcal{D}(\alpha_n)], \quad \mathcal{D}(\alpha_n) = \mathrm{e}^{-\alpha_n^2} \int_0^{\alpha_n} \mathrm{e}^{y^2}\, \mathrm{d}y, \tag{A.3a}$$

$$\alpha_n = \frac{\lambda_n}{2\zeta_s} - i\zeta_s, \tag{A.3b}$$

where we have used (3.16). Here $\mathcal{D}$ is *Dawson's integral*, as defined by Abramowitz & Stegun (1972, Section 7).

The Fourier series approach provides a useful solution for large τ, as the fast decay of the exponentials in (A.2) minimizes the number of terms that need be calculated. For small τ, we use the approach in Carrier & Pearson (1988, Section 2.3), wherein one expands the Laplace transform of the solution for large p, which corresponds to a series solution good for small τ.

Taking the Laplace transform of (2.8) subject to (A.1) yields a forced second-order ODE for the transform. Using Green's function approach to solve the problem and expanding the resulting expression for large transform variable p, we have the following:

$$\hat{C}_{\mathrm{w}}(x) = \frac{1}{p} - \frac{(1 - C_{\mathrm{T}})}{p \operatorname{erf} \zeta_s} \left[\operatorname{erf} \zeta_s (1 - x) + \frac{\hat{q}(x)}{2}\right], \tag{A.4a}$$

$$\hat{q}(x) \sim -4\zeta_s \mathrm{e}^{-\zeta_s^2} \sqrt{\frac{D_{\mathrm{w}}}{\pi p}} \sum_{n=0}^{\infty} (-1)^n [\mathrm{e}^{-(x+2n)\sqrt{p/D_{\mathrm{w}}}} - \mathrm{e}^{-(2-x+2n)\sqrt{p/D_{\mathrm{w}}}}]. \tag{A.4b}$$

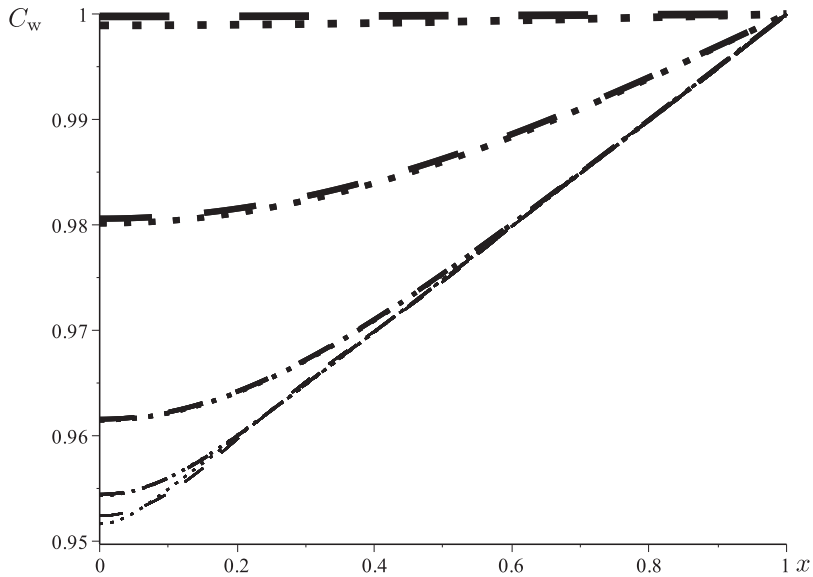

FIG. 8. C_w vs x for (in increasing order of thickness) $\tau = 3/7^3, 3/7^2, 3/7, 3, 21$. Dashed curves: C_w as given by (A.2) and (A.3). Dotted curves: C_w as given by (A.5).

Combining (A.4) and inverting, we have the following:

$$C_w(x,\tau) = 1 - \frac{(1-C_T)}{\operatorname{erf}\zeta_s}\left\{\operatorname{erf}\zeta_s(1-x) - 2\zeta_s e^{-\zeta_s^2}\sqrt{\frac{D_w}{\pi}}\sum_{n=0}^{\infty}(-1)^n \right.$$
$$\times\left[2\sqrt{\frac{\tau}{\pi}}\exp\left(-\frac{(x+2n)^2}{4D_w\tau}\right) - \frac{x+2n}{\sqrt{D_w}}\operatorname{erfc}\left(\frac{x+2n}{2\sqrt{D_w\tau}}\right)\right.$$
$$\left.\left. - 2\sqrt{\frac{\tau}{\pi}}\exp\left(-\frac{(2-x+2n)^2}{4D_w\tau}\right) + \frac{2-x+2n}{\sqrt{D_w}}\operatorname{erfc}\left(\frac{2-x+2n}{2\sqrt{D_w\tau}}\right)\right]\right\}. \qquad \text{(A.5)}$$

The two solution forms are compared in Fig. 8, which shows both the Fourier (long-τ) and Laplace (short-τ) series solutions together for various values of τ. Note the similarity between the two curves, with small differences appearing only for very small and large τ.

Appendix B. Nomenclature

B.1 *Variables and parameters*

The equation where a quantity first appears is listed, if appropriate.

A	constant in corner-layer solution (4.6)
$C(\cdot,t)$	concentration of ionic clusters (2.1a)
$\mathcal{D}(\alpha_n)$	Dawson's integral (A.3a)
$D(C)$	diffusion coefficient (2.1b)

p	Laplace transform variable (A.4a)
$\hat{q}(x)$	portion of Laplace series solution (A.4b)
$\Re(\cdot)$	real part (A.3a)
r	radius (6.1)
$s(t)$	front separating the dry and wet polymer regions
t	time
$u(\cdot)$	layer solution, written as deviation from C_{T} (4.2)
x	distance
y	dummy variable
$\mathcal{Z}$	the integers
z	intermediate-layer variable near front (3.9)
α_n	shifted eigenvalue (A.3b)
ζ	similarity variable (3.4)
η	internal-layer variable (4.2)
κ	perturbation parameter characterizing speed of transition and size of dry diffusion coefficient (2.1b)
λ_n	eigenvalue for series solutions (A.2)
τ	time after $t_{\max}$
ϕ_n	parameter in Fourier series solution (A.2)

B.2 *Other notation*

c	as a subscript, used to indicate the corner-layer solution (4.2)
d	as a subscript, used to indicate the dry polymer (2.1b)
max	as a subscript on t, used to indicate the time when the polymer saturates (3.3)
$n \in \mathcal{Z}$	as a subscript, used to index modes in the post-coalescence series solutions (A.2)
s	as a subscript on ζ, used to indicate the front separating the dry and wet polymer regions (3.4)
T	as a subscript on C, used to indicate the saturation concentration (2.1b)
w	as a subscript, used to indicate the wet polymer (2.1b)
0	as a subscript on r, used to indicate the post boundary (6.1)
*	as a subscript on D, used to indicate the scaled dry diffusion coefficient (2.6)
$>$	as a subscript on C, used to indicate the intermediate-layer solution in the wet region (3.9)
$\hat{}$	used to indicate the Laplace transform (A.4a)
$<$	as a subscript on C, used to indicate the intermediate-layer solution in the wet region (4.10)